Pacific Northwest
NATIONAL LABORATORY

PNNL-32031

Evaluation of PNNL Experimental Apparatus for Iodine Speciation Studies Using 14 MeV Neutrons

September 2021

James M Bowen
Christian C Cowles
Edward R Siciliano
Tracy A Ikenberry
Bethany M Lawler
Richard S Wittman
Katie A Wagner

U.S. DEPARTMENT OF ENERGY

Prepared for the U.S. Department of Energy
under Contract DE-AC05-76RL01830

DISCLAIMER

This report was prepared as an account of work sponsored by an agency of the United States Government. Neither the United States Government nor any agency thereof, nor Battelle Memorial Institute, nor any of their employees, makes **any warranty, express or implied, or assumes any legal liability or responsibility for the accuracy, completeness, or usefulness of any information, apparatus, product, or process disclosed, or represents that its use would not infringe privately owned rights**. Reference herein to any specific commercial product, process, or service by trade name, trademark, manufacturer, or otherwise does not necessarily constitute or imply its endorsement, recommendation, or favoring by the United States Government or any agency thereof, or Battelle Memorial Institute. The views and opinions of authors expressed herein do not necessarily state or reflect those of the United States Government or any agency thereof.

PACIFIC NORTHWEST NATIONAL LABORATORY
operated by
BATTELLE
for the
UNITED STATES DEPARTMENT OF ENERGY
under Contract DE-AC05-76RL01830

Printed in the United States of America

Available to DOE and DOE contractors from
the Office of Scientific and Technical Information,
P.O. Box 62, Oak Ridge, TN 37831-0062
www.osti.gov
ph: (865) 576-8401
fox: (865) 576-5728
email: reports@osti.gov

Available to the public from the National Technical Information Service
5301 Shawnee Rd., Alexandria, VA 22312
ph: (800) 553-NTIS (6847)
or (703) 605-6000
email: info@ntis.gov

Online ordering: http://www.ntis.gov

PNNL-32031

Evaluation of PNNL Experimental Apparatus for Iodine Speciation Studies Using 14 MeV Neutrons

September 2021

James M Bowen
Christian C Cowles
Edward R Siciliano
Tracy A Ikenberry
Bethany M Lawler
Richard S Wittman
Katie A Wagner

Prepared for
the U.S. Department of Energy
under Contract DE-AC05-76RL01830

Pacific Northwest National Laboratory
Richland, Washington 99354

Summary

In support of the National Nuclear Security Administration's Office of Conversion, experiments were conducted to determine the chemical form of iodine generated during production of molybdenum-99 using an aqueous homogeneous subcritical system. Comparisons between the neutrons used in the experimental apparatus and the production system allow for a higher-fidelity interpretation of experimental results and are accomplished by a series of evaluations described in this report. These evaluations of the PNNL experimental system can be applied to other types of aqueous homogeneous subcritical systems for use in interpreting results from experiments using a target material consisting of uranyl sulfate. Neutron current efficiencies, fission events, and deposited energy were evaluated per source neutron to allow for comparisons to other systems. The deposited energy will contribute to radiolysis of the target material, but the impact from neutron scattering and moderation is not adequately understood. The evaluations described in this report can be made compatible with other systems by modifying the target material composition providing flexibility in assessing multiple scenarios.

Acronyms and Abbreviations

DT	deuterium-tritium
DU	depleted uranium
LET	linear energy transfer
LEU	low enriched uranium
LSF	Low Scatter Facility
MCNP	Monte Carlo n-particle
PNNL	Pacific Northwest National Laboratory
ROI	region of interest
SHINE	SHINE Technologies, LLC

Contents

Summary ii
Acronyms and Abbreviations iii
1.0 Introduction 6
2.0 PNNL Experimental Setup 7
2.1 Evaluation of Neutron Currents 12
2.2 Energy Deposition 17
3.0 Radiolysis 19
4.0 Conclusions 21
5.0 References 22

Figures

Figure 1. PNNL's D711 Neutron Generator (Thermo Scientific™), center, on a platform in the Low-Scatter Facility. The LSF allows for >98% of neutrons to be at 14 MeV by minimizing room return. 7
Figure 2. Close up views of the tritiated target (a), the stainless-steel cooling cap (b), and the DT generator head (c). 8
Figure 3. Expanded view of the target solution holder. Optical windows on the sides allow for the coupling of a fiber optic cable that allows for image collection while operating the neutron generator. An optical port on the top is used as a light source. Two additional ports at the top are used to purge the headspace of any volatile fission gases post irradiation. 8
Figure 4. 3D MCNP geometry of the target holder secured to the DT generator head. 9
Figure 5. MCNP geometry of the target solution, target holder, and body of the DT generator. 9
Figure 6. Annotated MCNP geometry of PNNL's experimental setup with materials listed. 10
Figure 7. MCNP geometry of PNNL's experimental setup (left) with shaded red portion expanded (right) and showing neutron tracks. 11
Figure 8. View of the PNNL experimental setup and 1,000 particle histories. Different colors indicate energy lost during the reaction. 11
Figure 9. The full system neutron current efficiency showing the probability of a source neutron having a given energy when it enters and exits the system. 12
Figure 10. Neutron current efficiency and energy spectrum of the full system for each surface of the target solution. 13
Figure 11. Neutron current efficiency and energy spectrum of the full system for each surface of the target solution expanded to show neutron current efficiencies below 14 MeV. 13

Figure 12. Comparison of the neutron current efficiencies for neutrons entering the bottom of the target solution. 14
Figure 13. Comparison of the neutron current efficiencies for neutrons exiting the bottom of the target solution. 14
Figure 14. Comparison of the neutron current efficiencies for neutrons entering the sides of the target solution. 15
Figure 15. Comparison of the neutron current efficiencies for neutrons exiting the sides of the target solution. 15
Figure 16. Comparison of the neutron current efficiencies for neutrons entering the top of the target solution. 16
Figure 17. Comparison of the neutron current efficiencies for neutrons exiting the top of the target solution. 16
Figure 18. Energy deposited in the target material per source neutron for all reactions and fissions as determined by heating tallies 17
Figure 19. Comparison of fission events using DU (0% U-235) and LEU (19.75% U-235) in full systems. 18
Figure 20. Comparison of fission events using DU for full and bare systems and LEU for full systems on a logarithmic plot. 18
Figure 21. Variation of the radiolytic yield of the dominant radicals and the molecular species produced during irradiation of an acidic sulfate solution. Figure taken from reference (Youker et al., 2014). 20

Tables

Table 1. Neutron current efficiencies for regions of interest in the full system for all surfaces. 12
Table 2. Comparison of neutron current efficiencies for the bottom surface of the target material. 14
Table 3. Comparison of neutron current efficiencies for the side surface of the target material. 15
Table 4. Comparison of neutron current efficiencies for the top surface of the target material. 16
Table 5. Energy deposition efficiency (MeV per gram target material per source neutron) for all reactions and fission reactions and by ROI. 17
Table 6. Power deposited in the target material by all reactions, fission reactions, and non-fission reactions for a 200g target with a neutron emission rate of 2×10^{10} n/s. 17

1.0 Introduction

Pacific Northwest National Laboratory (PNNL) has conducted experiments to characterize the iodine produced during the irradiation of a subcritical uranyl sulfate target solution with 14 MeV neutrons produced by a deuterium-tritium (DT) reaction. Understanding the chemical form of iodine will guide iodine control measures to help protect worker safety, the environment, and public health. The experiments represented a scaled-down version of a system being evaluated for production of molybdenum-99. This aqueous homogeneous subcritical system will use 14 MeV neutrons produced by a DT neutron generator that become thermalized in the target solution. Despite both systems utilizing 14 MeV neutrons, the neutronics will be different for each due to total neutron production, flux, scattering, and other factors. Understanding these differences is of importance for correctly interpreting results from experiments and to guide iodine control measures.

This report describes PNNL's experimental setup, including the DT neutron generator, target solution, and target solution holder (target holder). Radiation transport models were used to evaluate the neutron currents and spectra at multiple surfaces of the target solution to inform on the moderating effects of the system and neutron leakage. Comparisons were made between a bare system with the target holder removed and the full system that includes scattering from the target holder and neutron generator. Energy deposited by induced fissions were compared to total energy deposited in the target solution from other scattering and absorption events. This deposited energy is expected to create radiolysis products that will affect chemistry and is briefly discussed.

2.0 PNNL Experimental Setup

PNNL operates a Thermo Scientific D711 14 MeV neutron generator, shown in Figure 1, that produces a flux of 10^9 n/cm^2/s in the center of the neutron generator head at full power, 3.0 mA beam current and 160 kV accelerating voltage, using DT reactions. The generator resides in the Low-Scatter Facility (LSF) that allows for >98% of the neutrons incident on the target to be at 14 MeV.

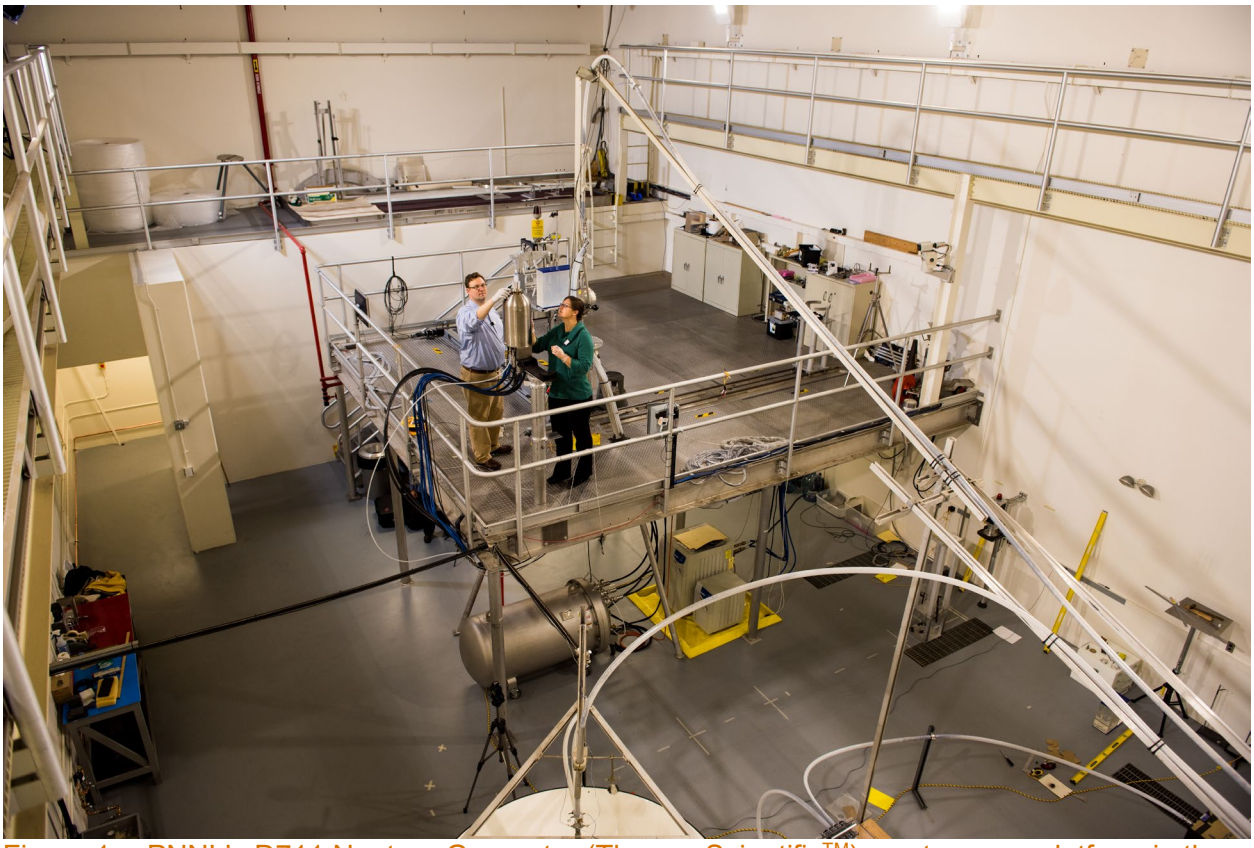


Figure 1. PNNL's D711 Neutron Generator (Thermo Scientific™), center, on a platform in the Low-Scatter Facility. The LSF allows for >98% of neutrons to be at 14 MeV by minimizing room return.

The head of the DT generator consists of a long "snout" containing the tritiated target covered by a stainless-steel cap to provide cooling water, shown in Figure 2. The stainless-steel cap and cooling water are the source of energy loss for the neutron beam. The target solution holder, shown in Figure 3, was fabricated from aluminum, to minimize dose rates from activation, with a silicon-based coating applied to protect the holder from corrosion of the acidic matrix. Optical windows on the side and a light source on the top allowed for collection of images during the irradiation and two ports allowed for a carrier gas to purge the head space following irradiations. The target holder was secured to the DT generator head using Teflon set screws.

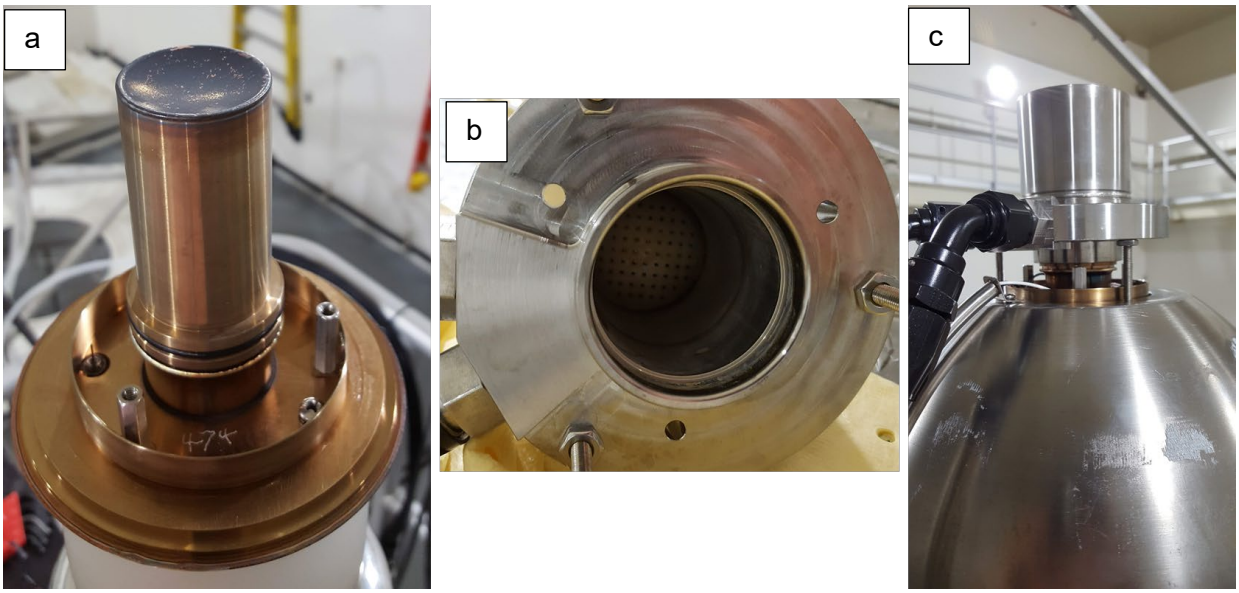


Figure 2. Close up views of the tritiated target (a), the stainless-steel cooling cap (b), and the DT generator head (c).

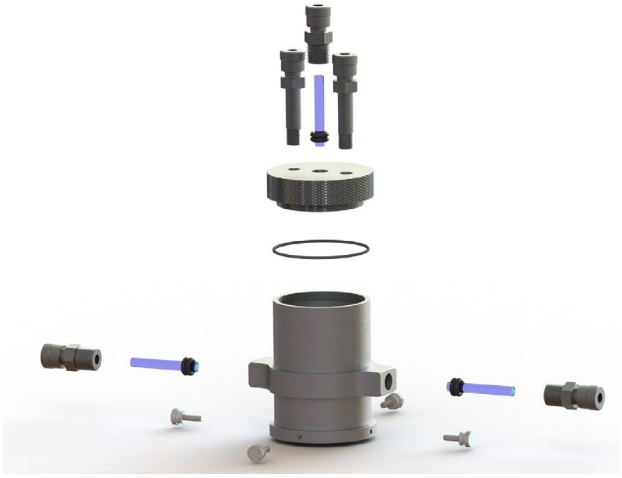


Figure 3. Expanded view of the target solution holder. Optical windows on the sides allow for the coupling of a fiber optic cable that allows for image collection while operating the neutron generator. An optical port on the top is used as a light source. Two additional ports at the top are used to purge the headspace of any volatile fission gases post irradiation.

Monte Carlo N-Particle code version 6.2 (MCNP6.2) (Werner 2017) was used to conduct simulations. The geometry used is shown in Figure 4, with an annotated view in Figure 5. A comparison of neutron current efficiency was completed for each boundary of the target solution. Since the ratio of fission cross sections at 14 MeV for U-235:U-238 is approximately 2:1, the target solution used depleted uranium (DU) instead of low-enriched uranium (LEU) to avoid criticality safety and safeguard accountability hazards for these experiments. A comparison of energy deposition, both total and fission induced, between the two materials is included.

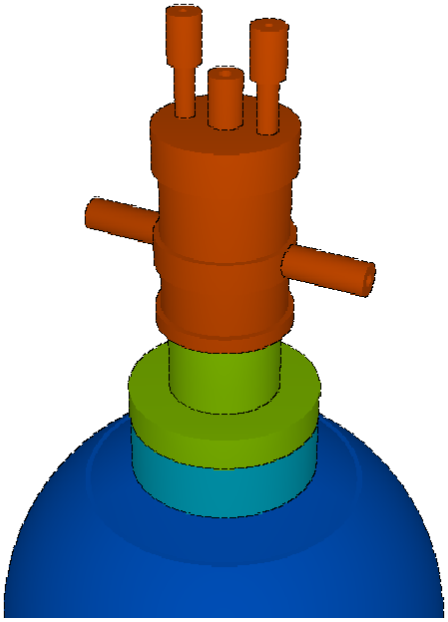


Figure 4. 3D MCNP geometry of the target holder secured to the DT generator head.

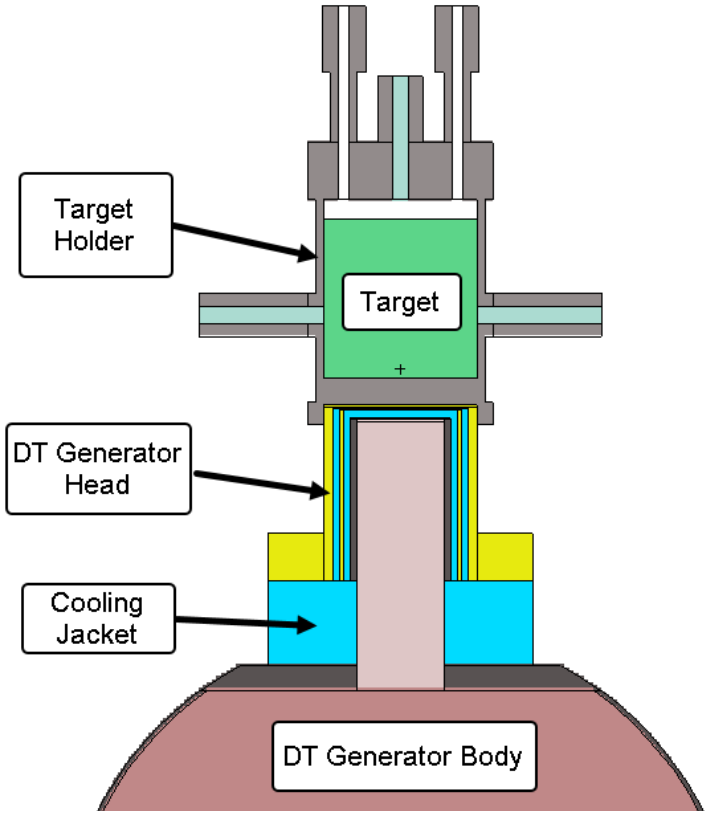


Figure 5. MCNP geometry of the target solution, target holder, and body of the DT generator.

The materials used for each component are shown in Figure 6. The neutron source was modeled as a thin disk, highlighted in the red box, with isotropic emission of neutrons. Because the neutrons are produced by accelerating deuterium and tritium ions at an embedded source of deuterium and tritium, the actual emission will be biased in the vertical direction. The isotropic emission of the neutrons from the source is a simplistic approach used in the modeling. The neutron track history is shown in Figure 7 as a closeup of the source disk. Figure 8 shows 1,000 neutrons tracked within the experimental setup.

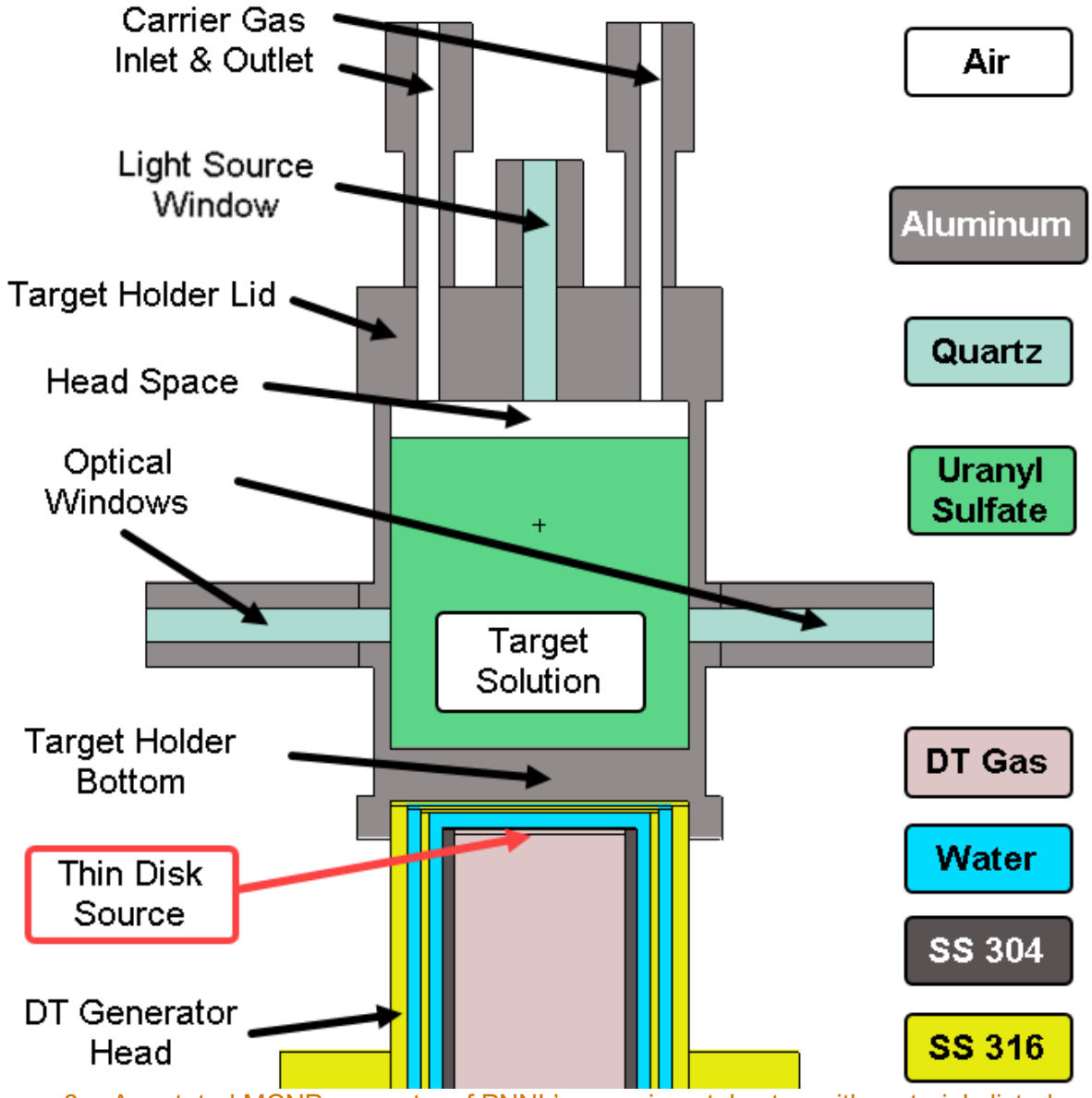


Figure 6. Annotated MCNP geometry of PNNL's experimental setup with materials listed.

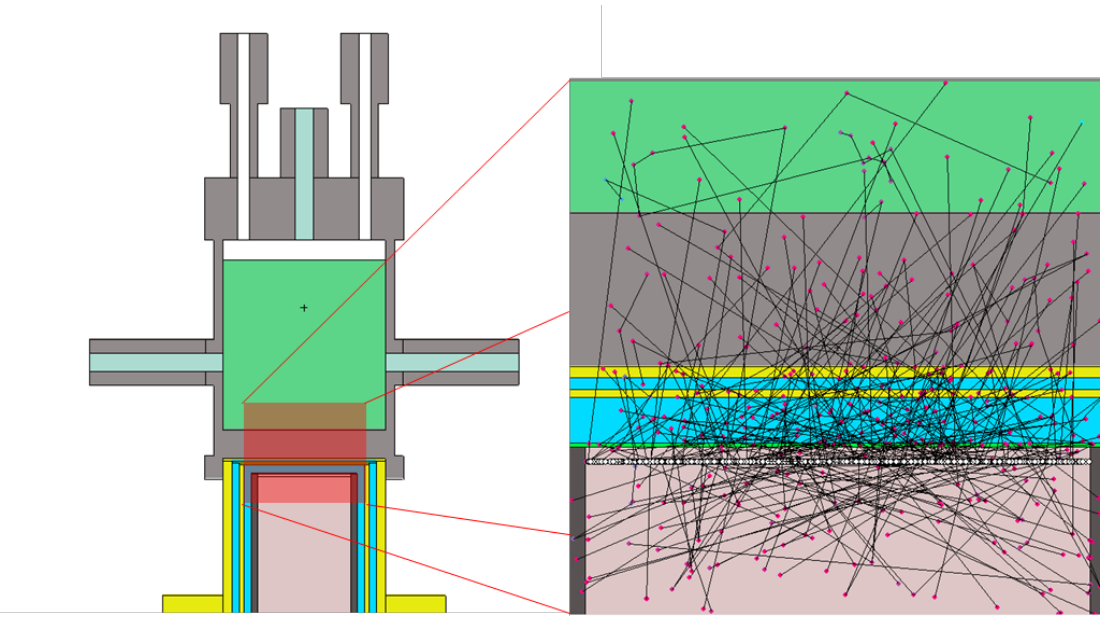


Figure 7. MCNP geometry of PNNL's experimental setup (left) with shaded red portion expanded (right) and showing neutron tracks.

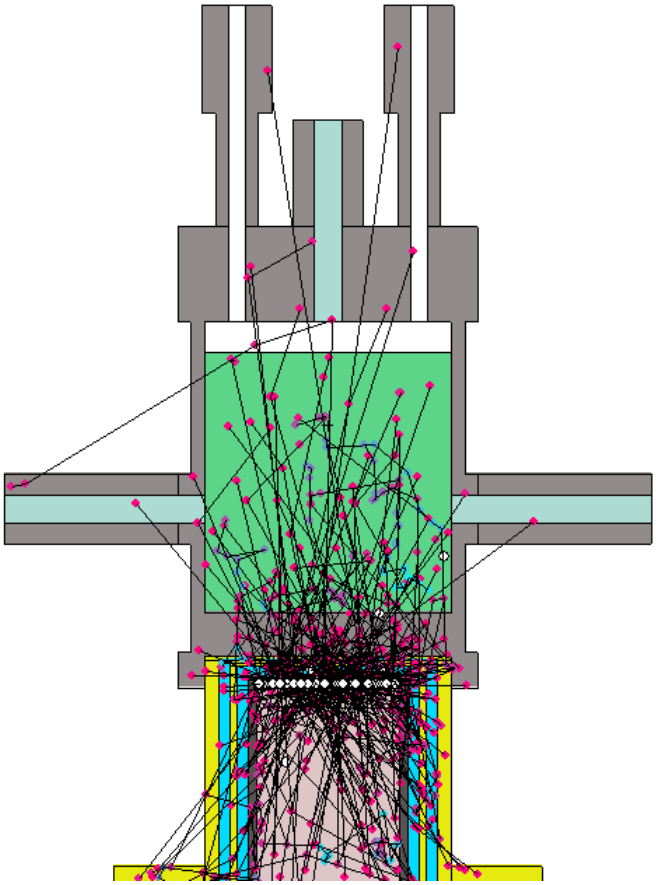


Figure 8. View of the PNNL experimental setup and 1,000 particle histories. Different colors indicate energy lost during the reaction.

2.1 Evaluation of Neutron Currents

The neutron currents per source neutron, referred to as the neutron current efficiency, of PNNL's experimental setup, utilizing an aqueous homogenous subcritical assembly consisting of a uranyl sulfate solution, were evaluated using MCNP6.2 (Werner 2017) to characterize the neutrons entering and exiting the system and their energies, shown in Figure 9 and Table 1 for the full system. This was conducted in PNNL's system using the D711 neutron generator for bare systems (geometries without the target holder) and full systems (geometries with the target holder) for each surface of the target solution. Evaluations of the full and bare systems allow for an understanding of how the target holder impacts the neutron spectrum. Evaluations used three regions of interest (ROI) for neutron energies: 0 – 2 MeV, 2 – 13.25 MeV, and 13.25 – 16 MeV (14 MeV). The differences, or loss, between the neutrons entering and exiting indicate unreacted neutrons in the 14 MeV ROI (positive) and moderated neutrons in the other ROI's (negative).

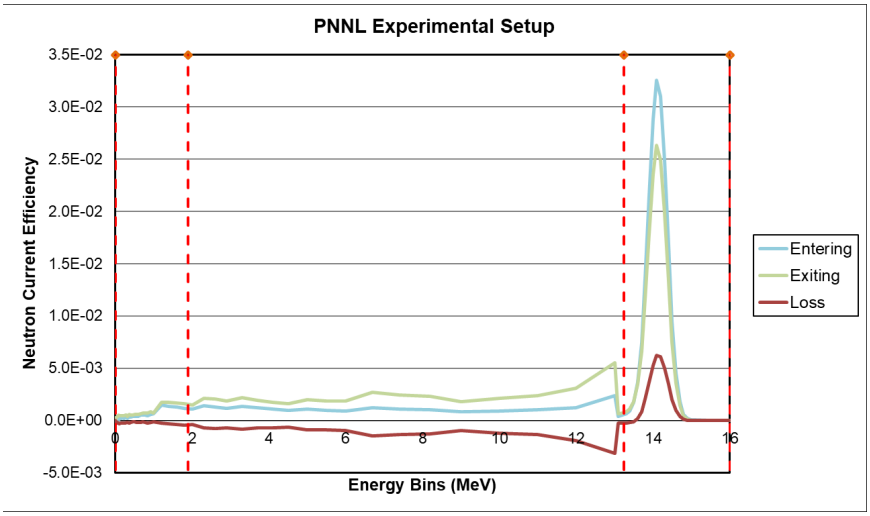


Figure 9. The full system neutron current efficiency showing the probability of a source neutron having a given energy when it enters and exits the system.

Table 1. Neutron current efficiencies for regions of interest in the full system for all surfaces.

	Total	ROI 0 - 2 MeV	ROI 2 - 13.25 MeV	ROI 13.25 - 16 MeV
Enter	23.80%	1.55%	2.28%	19.96%
Exit	23.51%	2.75%	4.40%	16.35%
Loss	0.29%	-1.20%	-2.12%	3.61%

Figure 10 and Figure 11 show the neutron current efficiencies for neutrons entering and exiting each surface of the target solution for the full system. In the 14 MeV region of interest, the primary peak is neutrons crossing the bottom boundary of target solution, followed by the neutrons exiting through the side boundary and then the top boundary. Neutrons exiting through the top boundary are those that did not interact, through scattering or absorption, with the target holder or target solution. As expected, there are none exiting the bottom or entering through the sides or the top in this ROI. Scattering of the source neutrons due to the presence of the target holder is indicated in Figure 11 for the 0 – 2 MeV and 2 – 13.25 MeV ROI's in pink.

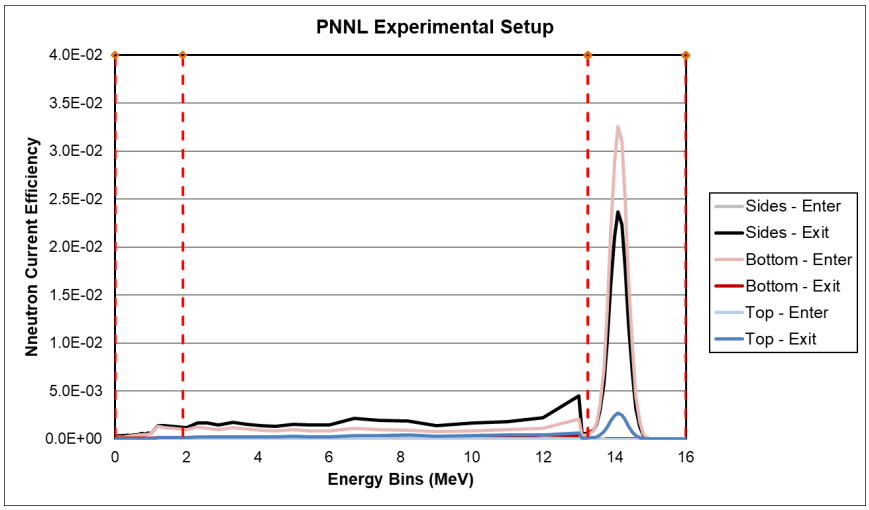


Figure 10. Neutron current efficiency and energy spectrum of the full system for each surface of the target solution.

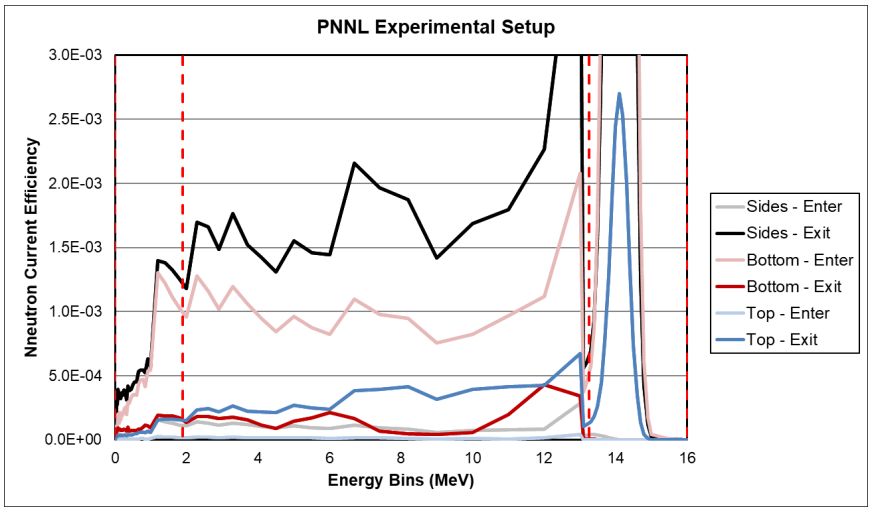


Figure 11. Neutron current efficiency and energy spectrum of the full system for each surface of the target solution expanded to show neutron current efficiencies below 14 MeV.

Given that the target holder is positioned on top of the DT neutron generator, the neutron current entering the bottom of the target solution represents the source of neutrons available to interact with the target material. The difference in neutron current efficiencies comparison shown in Figure 12 represents the scattering effects of the target holder. Fewer neutrons enter the target solution in the 14 MeV ROI for the full system in comparison to the bare system due to moderation caused by the aluminum target holder. The moderated neutrons, those in the other ROI's, show a higher population in the full system due to the presence of the target holder.

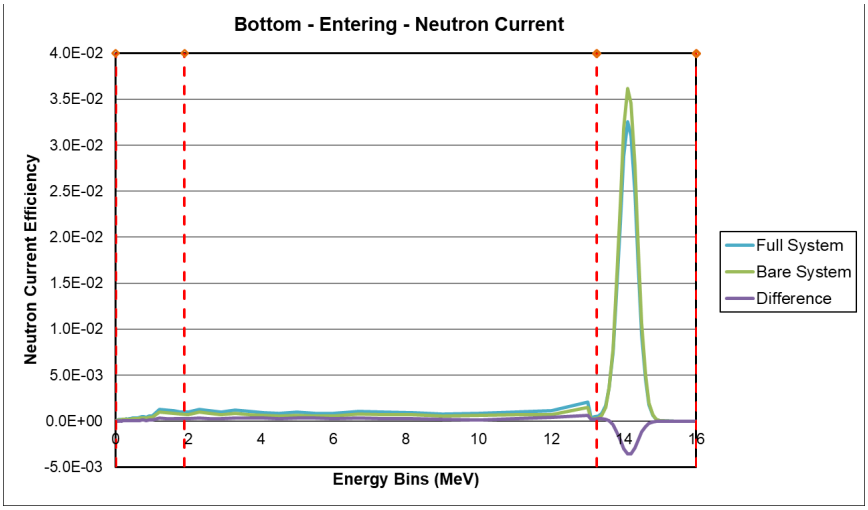


Figure 12. Comparison of the neutron current efficiencies for neutrons entering the bottom of the target solution.

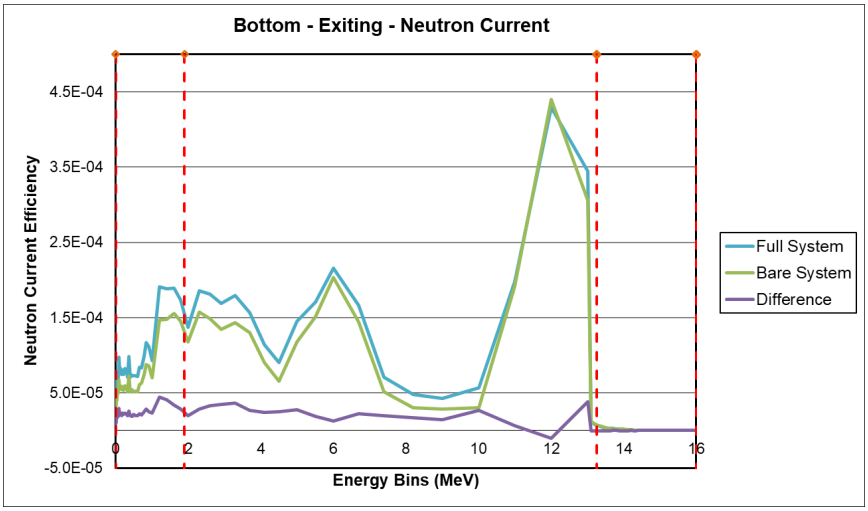


Figure 13. Comparison of the neutron current efficiencies for neutrons exiting the bottom of the target solution.

The 14 MeV ROI for neutrons exiting through the bottom surface is empty, as expected and shown in Figure 13. Table 2 shows that the presence of the target holder reduces the neutron inventory by approximately 1% total and 2% in the 14 MeV ROI.

Table 2. Comparison of neutron current efficiencies for the bottom surface of the target material.

	Total	ROI 0-2.05 MeV	ROI 2.05-13.25 MeV	ROI 13.25-16 MeV
Bottom Entering - Full	23.32%	1.34%	2.03%	19.94%
Bottom Entering - Bare	24.42%	1.05%	1.41%	21.97%
Bottom Exiting - Full	0.72%	0.42%	0.30%	0.00%
Bottom Exiting - Bare	0.57%	0.31%	0.26%	0.00%

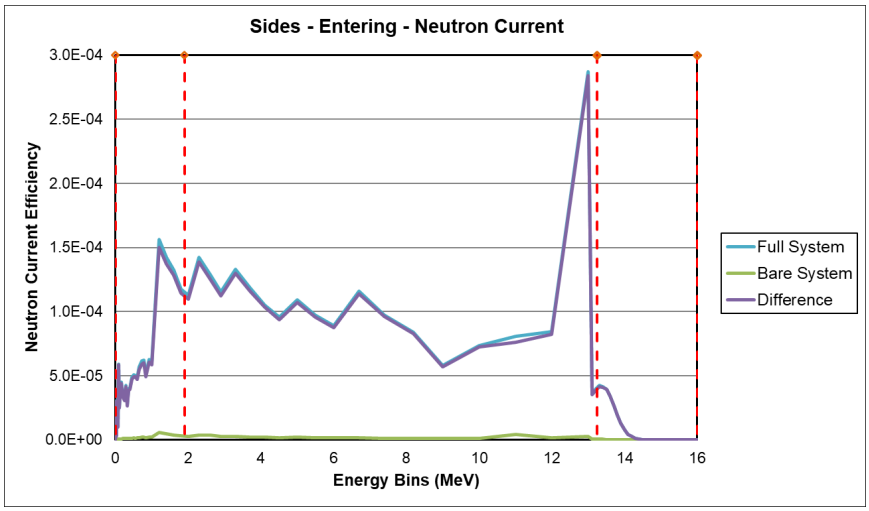


Figure 14. Comparison of the neutron current efficiencies for neutrons entering the sides of the target solution.

The limited number of neutrons, for all energies but particularly at 14 MeV, entering the sides of the target material for both the full and bare systems, shown in Figure 14 and Table 3, is consistent with the low-scatter environment of the LSF. Figure 15 shows that the sides of the target material are the surface that have the greatest loss of 14 MeV neutrons, though this number would likely be reduced slightly if the neutrons had a vertical emission bias. Greater leakage at moderated neutron energies for the sides than other surfaces is expected.

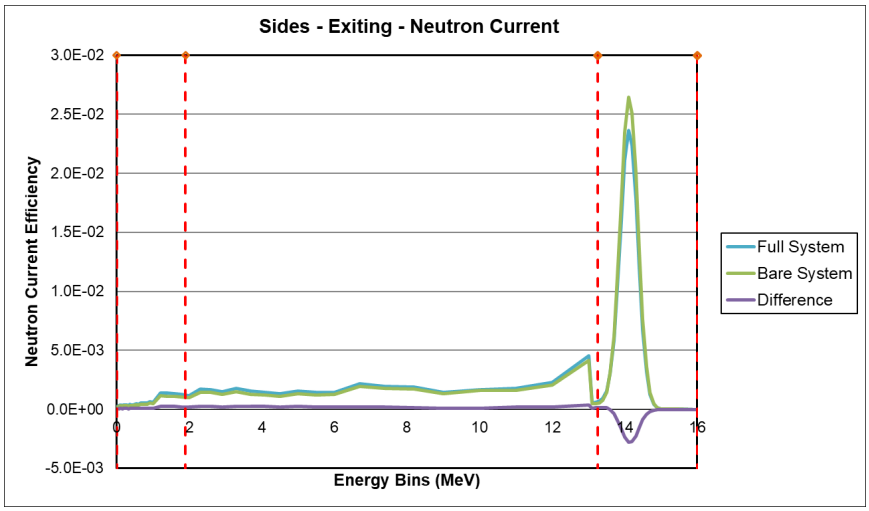


Figure 15. Comparison of the neutron current efficiencies for neutrons exiting the sides of the target solution.

Table 3. Comparison of neutron current efficiencies for the side surface of the target material.

	Total	ROI 0-2.05 MeV	ROI 2.05-13.25 MeV	ROI 13.25-16 MeV
Sides Entering - Full	0.41%	0.18%	0.21%	0.02%
Sides Entering - Bare	0.01%	0.01%	0.00%	0.00%
Sides Exiting - Full	20.22%	2.10%	3.49%	14.64%
Sides Exiting - Bare	20.99%	1.69%	3.07%	16.23%

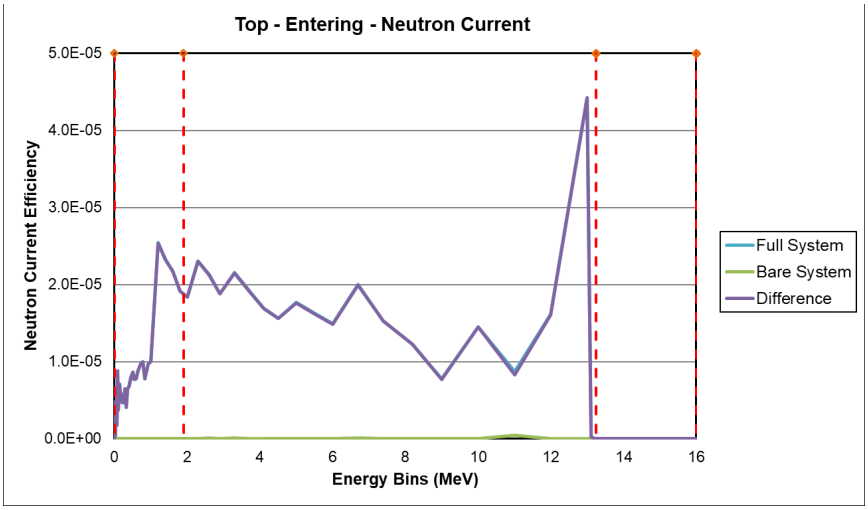


Figure 16. Comparison of the neutron current efficiencies for neutrons entering the top of the target solution.

Figure 16 and Table 4 show that neutrons are not entering the system from the top of the target material with a minimal exception for when scattered by the target holder. The 14 MeV neutrons shown in Figure 17 represent unattenuated neutrons that did not interact with the target holder, for the full system, or the target material, for both systems.

Table 4. Comparison of neutron current efficiencies for the top surface of the target material.

	Total	ROI 0-2.05 MeV	ROI 2.05-13.25 MeV	ROI 13.25-16 MeV
Top Entering - Full	0.06%	0.03%	0.03%	0.00%
Top Entering - Bare	0.00%	0.00%	0.00%	0.00%
Top Exiting - Full	2.57%	0.24%	0.62%	1.71%
Top Exiting - Bare	2.57%	0.19%	0.56%	1.82%

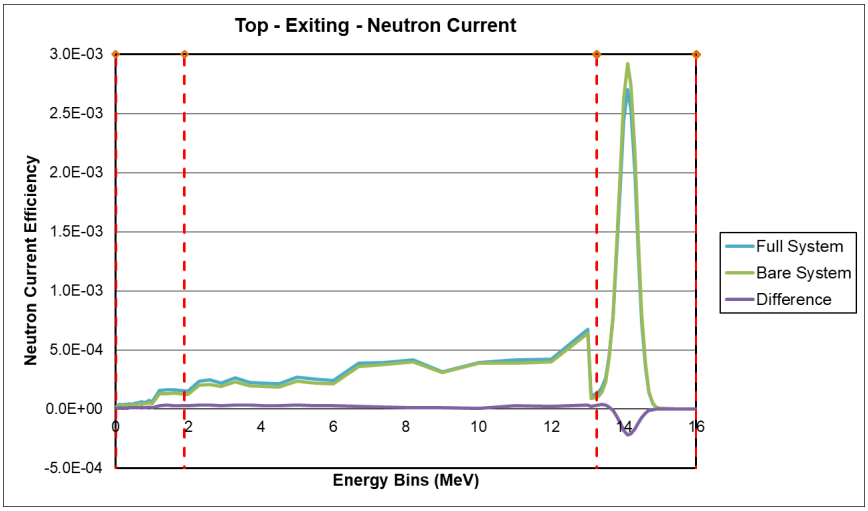


Figure 17. Comparison of the neutron current efficiencies for neutrons exiting the top of the target solution.

2.2 Energy Deposition

The energy deposited by all reactions (F6 tally) and fission reactions (F7 tally) was determined per source neutron, shown in Figure 18 and tabulated in Table 5. Significant energy deposition comes from the fission, but other reactions, such as neutron scattering events and decay from activated components of the target material such as sulfur, contribute most of the energy deposited. This energy is likely to affect the chemistry through production of radiolytic products. Total power for PNNL's experimental setup is shown in Table 6. These values can be used to compare PNNL's experimental setup to other systems using the same target material.

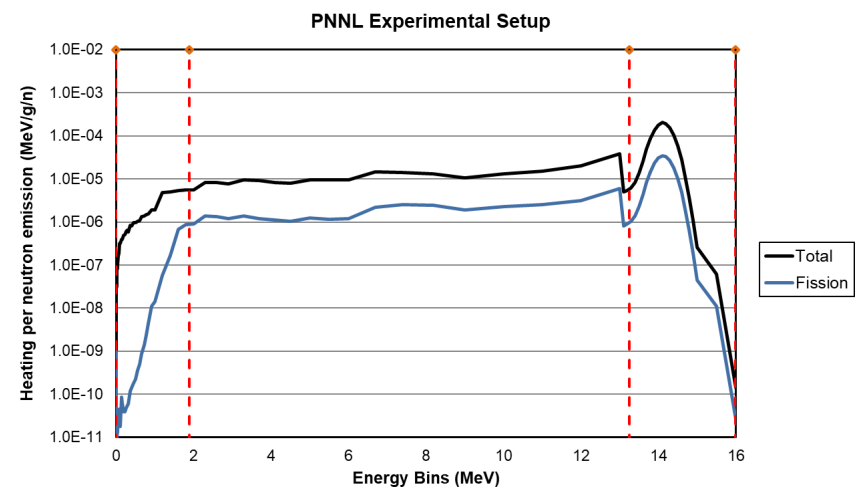


Figure 18. Energy deposited in the target material per source neutron for all reactions and fissions as determined by heating tallies

Table 5. Energy deposition efficiency (MeV per gram target material per source neutron) for all reactions and fission reactions and by ROI.

	Total	ROI 0-2.05 MeV	ROI 2.05-13.25 MeV	ROI 13.25-16 MeV
All Reactions	0.001537	4.67E-05	2.43E-04	1.25E-03
Fission	0.000256	2.73E-06	3.79E-05	2.15E-04

Table 6. Power deposited in the target material by all reactions, fission reactions, and non-fission reactions for a 200g target with a neutron emission rate of 2×10^{10} n/s.

All Reactions (W)	9.85E-04
Fission (W)	1.64E-04
Non-Fission (W)	8.21E-04

Since DU was utilized in PNNL's experimental setup to avoid criticality safety issues and safeguard accountability tracking, a comparison was modeled using 19.75% LEU. These comparisons, shown on a linear plot in Figure 19 to highlight the slight differences at 14 MeV and on a logarithmic plot in Figure 20 to highlight the differences at lower energies, indicate the most significant contribution to fission comes below 2 MeV. In a system with more thermalized neutrons, this contribution is expected to increase between DU and LEU target material.

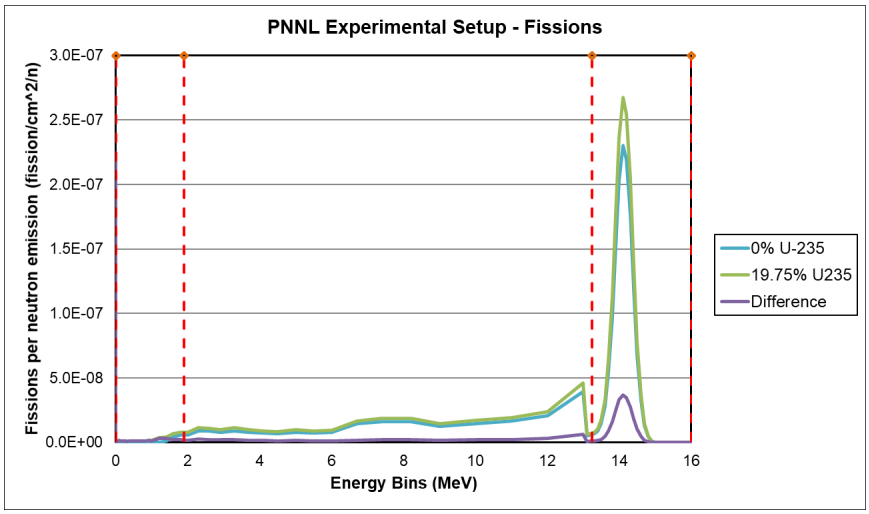


Figure 19. Comparison of fission events using DU (0% U-235) and LEU (19.75% U-235) in full systems.

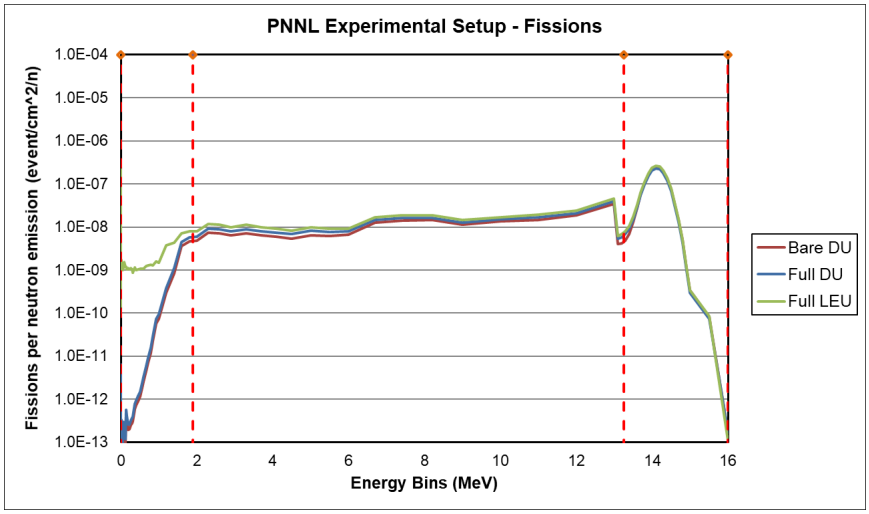


Figure 20. Comparison of fission events using DU for full and bare systems and LEU for full systems on a logarithmic plot.

3.0 Radiolysis

Radiolysis is an important factor to consider in the operation of aqueous systems. The radiolysis of water, a common process that results in a large number of radiolytic products, creates both molecular and radical species, such as H_2O^* or *OH. These in turn react with each other and other compounds in solution (Choppin, Liljenzin and Rydberg 2002). These interactions can lead to the formation of compounds that can inhibit the performance of the system, such as the evolution of H_2O_2 or precipitates, and affect the chemical form of system constituents, such as the fission products like iodine. It is important then to understand how irradiation affects the generation of these products.

Multiple studies have investigated the effect of electrons, protons, and alpha particles on aqueous radiolysis, but almost none on direct radiolytic effects of uncharged particles. This leads to difficulties when modeling the radiolytic effects during irradiation, as the SHINE Technologies, LLC (SHINE) subcritical system uses an irradiating beam comprised of 14 MeV neutrons produced by a DT neutron generator (Pardo et al., 2021).

The creation of radiolytic products is dependent on the LET (linear energy transfer) of the irradiating particle (Lane et al., 1958). It has been shown that low LET particles tend to produce fewer molecular products than high LET particles (Youker et al., 2014). Figure 21 shows the relationship between LET and radiolytic products. The particles studied were charged, however, which makes direct comparison difficult.

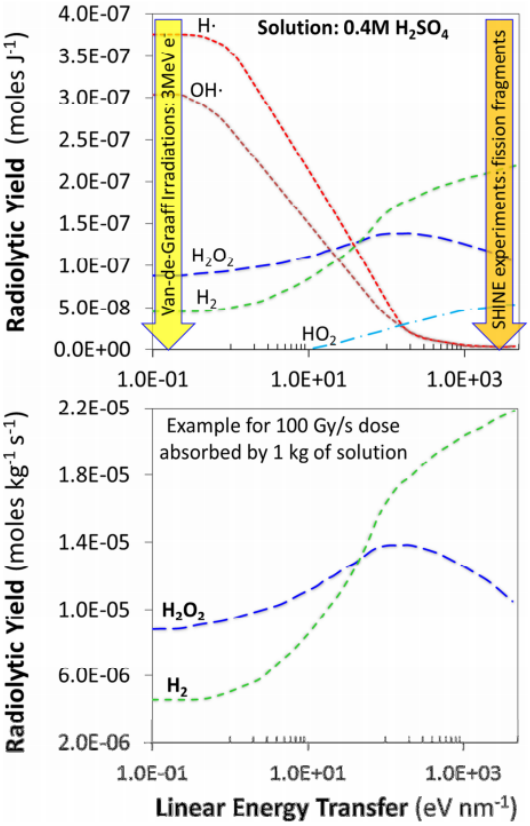


Figure 21. Variation of the radiolytic yield of the dominant radicals and the molecular species produced during irradiation of an acidic sulfate solution. Figure taken from reference (Youker et al., 2014).

Some evidence suggests that other, better characterized, low LET irradiation systems may be useful in modeling. Irradiations of uranyl sulfate solutions under similar conditions to those found in the SHINE aqueous homogenous subcritical system do show the evolution of both hydrogen and nitrogen gases (Youker et al., 2016) which supports the expected evolution of radiolytic products from a low LET particle irradiation. Van de Graff irradiations, which utilize low LET particles, have also been studied and display similar evolution of gases (Kalensky, Brossard, and Tkac, 2019; Kalensky et al., 2012). However, Lane et al. (1958) states that only 2% of the hydrogen gas generated in an aqueous homogenous system, like SHINE, can be attributed to neutrons, with approximately 96% of the H_2 gas formation is attributed to fission product recoil.

4.0 Conclusions

A series of neutron current efficiencies were produced to evaluate the neutron current and energy spectrum at multiple surface boundaries of the target solution per source neutron. Normalizing these values to the source neutron allow for quick comparisons to other systems for interpreting experimental results. Energy deposition was evaluated for contributions by fission and other reactions, such as neutron scattering and decay of activation products, for the energy deposited per unit material per source neutron. The energy deposited into the target material is likely to produce radiolytic products that could affect the chemical composition of the fission products. Radiolytic effects have been studied extensively for charged particles, but more research on neutron-induced radiolysis would improve fidelity when making comparisons between PNNL's system and others.

The evaluations performed for the PNNL experimental setup could be used to complete neutron energy comparisons between PNNL's system and other aqueous homogeneous subcritical systems using the same target material. These evaluations can be made compatible for use in other systems by modifying the target material definitions, such as the composition or density (to simulate different sized targets), in the input file used. Using H_2 gas formation as a surrogate for overall aqueous radiolytic effects indicates that the most effective evaluation for radiolysis between systems is a comparison of energy deposited in the target material.

5.0 References

Choppin, G., J. Liljenzin, and J. Rydberg. 2002. Radiochemistry and Nuclear Chemistry. Woburn, MA: Butterworth-Heinemann.

Kalensky, M., T. Brossard, and P. Tkac. 2019. *Low Let Irraditions of Uranyl Sulfate Solutions in the Absence and Presence of Fe^{+2} and Fe^{+3} Ions*. ANL-19/44. Chicago: Argonne National Laboratory. http://ww.osti.gov/scitech/.

Kalensky, M., S. Chemerisov, A. Youker, A. Hebden, P. Tkac, V. Makarashvili, E. Krahn, J. Krebs, K. Quigley, R. Lowe, D. Bowers, S. Niak, D. Graczyk, V. Sullican, A. Bakel, and G. Vandegrift. 2012. *Radiolysis of Nitrate and Sulfate Solutions*. ANL/CSE-13/23. Chicago: Argonne National Laboratory. http://ww.osti.gov/scitech/.

Lane, J., H.G. MacPherson, and F. Maslan. 1958. “Properties of Aqueous Fuel Solutions.” In *Fluid Fuel Reactors*, 85-127. Addison-Wesley Publishing Company, Inc.

Pardo L., D. Pérez, D. Lorenzo, and C. Brayner de Oliveira Lira. 2021. “Coupled multi-physics simulation for the evaluation of an accelerator-driven Aqueous Homogeneous Subcritical System for medical isotope production.” *Progress in Nuclear Energy*, 134 (April): 103692. https://doi.org/10.1016/j.pnucene.2021.103692.

Werner, C.J. (editor). 2017. "MCNP Users Manual - Code Version 6.2", LA-UR-17-29981

Youker, A., J. Jerden, M. Kalensky, K. Quigley, C. Jonah, S. Chemerisov, and G. Vandegrift. 2014. *Peroxide Formation, Destruction, and Precipitation in Uranyl Sulfate Solutions: Simple Addition and Radiolytically Induced Formation*. ANL/CSE-14/35. Chicago: Argonne National Laboratory. http://ww.osti.gov/scitech/.

Youker, A., M. Kalensky, S. Chemerisov, and J. Schneider. 2016. *Micro-SHINE Uranyl Sulfate Irradiations at the Linac*. ANL/NE-16/20. Chicago: Argonne National Laboratory. http://ww.osti.gov/scitech/.

Pacific Northwest National Laboratory

902 Battelle Boulevard
P.O. Box 999
Richland, WA 99354
1-888-375-PNNL (7665)

www.pnnl.gov